Numerical Simulation of the Stress-strain Behavior of Polymeric Fibers for Mooring Offshore Structures

Daniel M. Cruz[1,3], Marcelo A. Barreto[2,3], Larissa B. Zangalli[3], Felipe T. Stumpf[1], Jakson M. Vassoler[1], Carlos E. M. Guilherme[2]

[1]*Department of Mechanical Engineering, Federal University of Rio Grande do Sul*
Rua Sarmento Leite, 425, Centro Historico, Porto Alegre, 90050-170, Rio Grande do Sul, Brazil
daniel.cruz@ufrgs.br, felipe.stumpf@ufrgs.br, jmvassoler@ufrgs.br
[2]*Engineering School, Federal University of Rio Grande*
Avenida Itália, km 8, Carreiros, Rio Grande, 96203-000, Rio Grande do Sul, Brazil
marcelobarretobm@gmail.com, carlosguilherme@furg.br
[3]*Tecnofibers Desenvolvimento e Tecnologia LTDA*
Rua Doutor Hermes Atilio Mariani, 438, Cidade Nova, Itajaí, 88308-030, Santa Catarina, Brazil
larissa@tecnofibers.com

Abstract. Polyester fibers have been used in offshore mooring due to their excellent mechanical properties, resistance to marine environments, and relatively low cost. However, its mechanical behavior still needs further investigation since its working environment is subject to adverse conditions that can magnify inelastic behaviors. Thus, this work focuses on the characterization of components of this material according to different levels of construction. Multifilaments and sub-ropes were numerically simulated based on the Modified Yeoh strain energy model. The simulation parameters were adjusted using experimental data from cyclic tests, and the results were then compared with the experimental data. The numerical simulations demonstrated good agreement, with an average error of approximately 1.3% for both multifilaments and sub-ropes. Furthermore, the study identified dissimilarities in constitutive behavior between them due to the twisting and braiding involved in sub-rope construction. These findings suggest the possibility of developing a formation law that can predict the constitutive behavior of sub-ropes based on the numerical simulation results obtained for multifilaments. Such correlation could prove advantageous in optimizing material performance and construction methods for offshore moorings utilizing polyester fibers. However, it's important to conduct further studies to establish the precise correlation between both behaviors under different manufacturing conditions.

Keywords: Offshore mooring, Ultra deep-water, Constitutive model, Synthetic fibers, Strain energy function.

1 Introduction

In recent decades, polymeric materials have replaced classic engineering materials and shown promise in various applications, such as ropes for climbing and rescue operations (Horn et al. [1], Leal et al. [2]), surgical sutures (Pillai and Sharma [3], Chu [4], Tummalapalli et al. [5]), and concrete reinforcement to enhance tensile strength (Gupta et al. [6], Huang et al. [7]). These materials have also found use in reinforcement applications for ballistic protection (Tam et al. [8], Nurazzi et al. [9]) and offshore moorings (Del Vecchio [10]).

With a particular focus on the offshore sector, Del Vecchio [10] is a reference work that replaced steel catenaries with a Taut-Leg mooring system made of synthetic polyester fibers. This context has enabled the study and advancement of various synthetic fibers. To this day, polyester fibers remain prominent in mooring systems due to their excellent mechanical properties, low specific weight, resistance to the marine environment, and relatively low cost. Numerous works in the literature have addressed the use of polyester for offshore moorings, with studies on its properties dating back to the 1990s and continuing to the present day (Del Vecchio [10], Petruska et al. [11], Huang et al. [12], Weller et al. [13], Aqdam et al. [14], Saidpour et al. [15], Xu et al. [16]).

The development of numerical simulations has accompanied the evolution of polyester's use in the offshore sector. Many studies in the literature have numerically approached the material and tying systems (Beltran and Williamson [17], Ouarhim et al. [18], Amaechi et al. [19], da Cruz et al. [20]). However, simulating polymeric materials in numerical approaches presents challenges due to their viscoelastic characteristics and material and

geometric nonlinearities. Moreover, conducting experimental studies at the rope level is costly, making multifilament studies more common. Nevertheless, these multifilament studies may help predict parameters in numerical simulations through correlations between multifilaments and ropes.

The objective of this work is to simulate the constitutive behavior (stress-strain) of polyester fibers at two different construction levels: multifilaments and sub-ropes. To achieve this objective, numerical simulations will be performed for a load cycle involving loading and unloading (hysteresis), and the results will be adjusted using experimental data.

The numerical simulation routine follows the approach of Simo and Hughes [21], which addresses stress-strain relationships using tensors and mathematical definitions related to solid mechanics. The strain energy function is a crucial aspect of the numerical simulation, and for this study, the Modified Yeoh model will be used.

With the obtained results, we aim to analyze the correlations and potential observations of the results and model constants. By comparing the constitutive behaviors and simulation results for each construction level, it may be possible, with appropriate adjustments, to predict the constitutive behavior of different construction levels based on the results obtained from multifilament simulations.

2 Materials and methods

2.1 Material specification

The material used in this work is the polyester SFS5202, specifically used for offshore mooring applications. The material has a specific mass of 1.38 g/cm³ and a linear density of 2000 denier (2200 dtex) for multifilament. The samples are manufactured at two different construction levels: multifilament base material and constructed sub-rope. Figure 1 illustrates the construction levels and shows the multifilament and sub-rope samples.

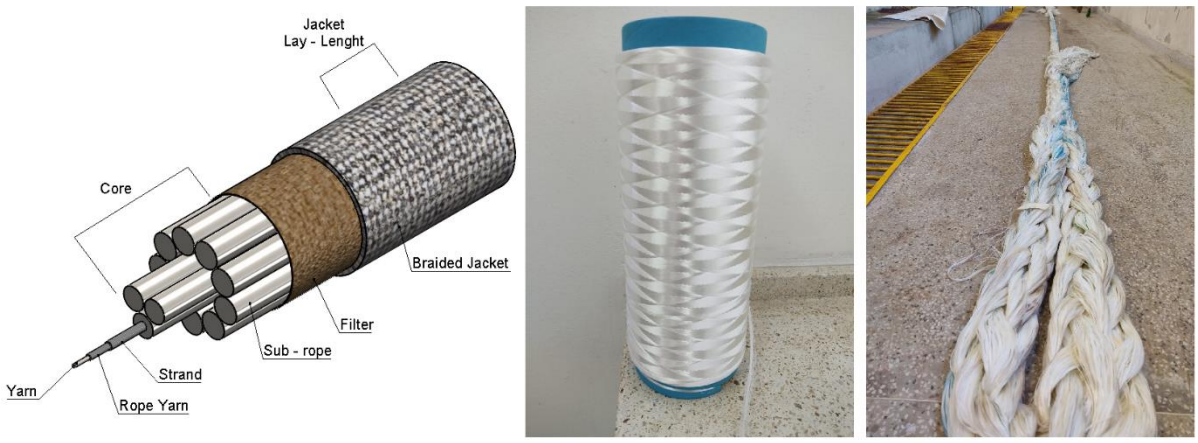

Figure 1. Rope exploded parts (left), spool for multifilament samples (center), sub-rope sample (right)

2.2 Experimental characterization

The numerical simulation incorporates experimental data from the charge and discharge cycle, which relies on the multifilament/sub-rope breaking load. The sub-rope has a Minimum Breaking Strength (MBS) of 1470kN, while the multifilament undergoes an experimental test to determine its linear density and tensile strength.

To conduct these tests, the linear density measurements were performed following ASTM D1577 [22] guidelines, using a precision scale. Each specimen was given 9 minutes for stabilization before recording its mass. The rupture test (Yarn Break Load, YBL) was carried out in accordance with the ISO 2062 [23] standard. Specimens with a useful length of 500 mm were subjected to an extension rate of 250 mm/min to obtain the resistance to rupture of multifilaments in Newtons.

Regarding the loading and unloading data used as a reference for the numerical simulations, it corresponds to the 10th load cycle as per the procedural protocol presented by da Cruz et al. [24]. The experimental reference

data corresponds to the last cycle conducted in a sine wave, with a lower limit of 20% and an upper limit of 50% of the breaking load, at a frequency of 6.25 mHz (160 seconds per cycle).

2.3 Mathematical and tensor description for the simulation

The numerical code was based on Simo and Hughes [21] and implemented by Cruz [25], being developed in MATLAB. The mathematical description was developed based on the theory of elasticity, continuum mechanics and the characteristics of the material worked.

For a body $\Omega \subset \mathbb{R}^3$, subjected to a finite deformation $\varphi : \Omega \to \mathbb{R}^3$, define the deformation gradient $\boldsymbol{F} = \partial\varphi(\boldsymbol{X})/\partial\boldsymbol{X}$ with the Jacobian $J = \det \boldsymbol{F} > 0$, where $\boldsymbol{X}$ is the material point in the reference, undeformed configuration. The strain gradient $\boldsymbol{F}$ can be decomposed multiplicatively, as shown in eq. (1), Flory [26]. Where $\widehat{\boldsymbol{F}}$ refers to the volumetric part with $\det \widehat{\boldsymbol{F}} = \det \boldsymbol{F} = J$, and $\overline{\boldsymbol{F}}$ refers to the isochoric part with $\det \overline{\boldsymbol{F}} = 1$, respectively defined in eq. (2) and eq. (3). ($\boldsymbol{I}$ corresponds to the identity matrix).

$$\boldsymbol{F} = \widehat{\boldsymbol{F}}\overline{\boldsymbol{F}} \tag{1}$$

$$\widehat{\boldsymbol{F}} = J^{1/3}\boldsymbol{I} \tag{2}$$

$$\overline{\boldsymbol{F}} = J^{-1/3}\boldsymbol{F} \tag{3}$$

From eq. (1), the right Cauchy-Green tensor in an isochoric parcel ($\overline{\boldsymbol{C}}$) is written as eq. (4). Since $\det \overline{\boldsymbol{C}} = 1$ and $\boldsymbol{C} = \boldsymbol{F}^T\boldsymbol{F}$, determine the invariants of $\overline{\boldsymbol{C}}$, in eq. (5), (6) and (7).

$$\overline{\boldsymbol{C}} = \overline{\boldsymbol{F}}^T\overline{\boldsymbol{F}} = J^{-2/3}\boldsymbol{C} \tag{4}$$

$$\overline{I_1} = \operatorname{tr} \overline{\boldsymbol{C}} \tag{5}$$

$$\overline{I_2} = \frac{1}{2}\left((\operatorname{tr} \overline{\boldsymbol{C}})^{\boldsymbol{2}} - \operatorname{tr} \overline{\boldsymbol{C}}^{\boldsymbol{2}}\right) \tag{6}$$

$$\overline{I_3} = \det \overline{\boldsymbol{C}} = 1 \tag{7}$$

Based on Simo and Hughes [21], an internal variable ($\boldsymbol{H}$) is created dependent on the material properties (τ_i), the time step (Δt_n) and the Piola-Kirchhoff stress tensor ($\tilde{\boldsymbol{S}}$), eq. (8). Thus, the operation counts on current time $n+1$, and previous time n indicated in the subscripts.

$$\boldsymbol{H}_{n+1} = \exp(-\Delta t_n/\tau_i)\boldsymbol{H}_n + \exp(-\Delta t_n/2\tau_i)\left(\tilde{\boldsymbol{S}}_{n+1} - \tilde{\boldsymbol{S}}_n\right) \tag{8}$$

The second Piola-Kirchhoff stress tensor ($\boldsymbol{S}$) is defined in numerical modeling according to eq. (9). This expression allows to obtain the Kirchhoff stress update equation through the mathematical model and strain and stress tensors and constitutes the counterpart as the spatial description of the updated formula. In the terms that appear, $\boldsymbol{I}$ is the identity matrix, $\boldsymbol{C}$ is the Cauchy-Green tensor on the right (which when it assumes the isochoric form gives rise to $\tilde{\boldsymbol{S}}$) and W refers to the energy function used. Section 2.4 is devoted to the strain energy model.

$$\boldsymbol{S} = 2\left[\frac{\partial W}{\partial I_1} + \frac{\partial W}{\partial I_2}\right]\boldsymbol{I} - 2\frac{\partial W}{\partial I_2}\boldsymbol{C} + 2\frac{\partial W}{\partial I_3}I_3\boldsymbol{C}^{-1} \tag{9}$$

An incremental deformation matrix is defined. This allows calculating the left ($\boldsymbol{B}$) and right ($\boldsymbol{C}$) Cauchy-Green strain tensors, operating with the strain matrix ($\boldsymbol{F}$) and its transposition according to continuum mechanics.

A deviation function equation is calculated both for the second Piola-Kirchhoff stress tensor ($\boldsymbol{S}$) and for the created variable ($\boldsymbol{H}$). Equation (10) shows the mathematical form of calculating this deviation function. It is also noteworthy that the operation between square brackets of eq. (10) is an inner product, which can be defined as the trace of the inverse of ■ with $\boldsymbol{C}$.

$$DEV_{n+1}[\blacksquare] = (\blacksquare) - \frac{1}{3}[(\blacksquare) : \boldsymbol{C}_{n+1}]\boldsymbol{C}_{n+1}^{-1} \tag{10}$$

The deviation functions associated with the system stiffness model provide a final stress matrix, indicated in eq. (11), where '°' indicates the deviation function. Simo and Hughes [21] also define that $\gamma_\infty = \gamma - 1$, where corresponds to a portion of the model's stiffness, rewriting eq. (11) in eq. (12).

$$\boldsymbol{S}_{final} = \gamma_\infty \cdot \boldsymbol{S}^{\circ}_{n+1} + \gamma \cdot \boldsymbol{H}^{\circ}_{n+1} \tag{11}$$

$$\boldsymbol{S}_{final} = (\gamma - 1) \cdot \boldsymbol{S}^{\circ}_{n+1} + \gamma \cdot \boldsymbol{H}^{\circ}_{n+1} \tag{12}$$

For the final stress expression, as the second Piola-Kirchhoff tensor is not feasible to be compared, a stress transformation is performed, which allows comparing the results. Thus, the Kirchhoff stress tensor (spatial) is calculated through the standard transformation (push-forward), eq. (13). With the stress already transformed, it is possible to extract strain and stress for plotting.

$$\boldsymbol{\sigma}_{n+1} = \boldsymbol{F}_{n+1}\boldsymbol{S}_{final}\boldsymbol{F}_{n+1}^{T} \tag{13}$$

2.4 Hyperelastic Strain Energy Models

Hyperelastic models are particularly well-suited for highly deformable elastic materials. The hyperelastic material, also known as Green's elastic material, according to Holzapfel [27], postulates the existence of a specific strain energy function W, commonly referred to as Helmholtz free energy. This function can be described for homogeneous and isotropic materials as a function of the strain invariants, $W(I_1, I_2, I_3)$. Another simplification occurs when considering incompressible materials, where the third invariant of the tensor is unity. This approach is applicable to numerous polymeric materials, including polyester. Therefore, in this study, we work with hyperelastic models suitable for isotropic, homogeneous, and incompressible materials.

In the literature, there are several hyperelastic models for strain energy, broadly categorized into two groups: phenomenological models and micromechanical models. For this particular study, the model chosen is the Modified Yeoh model eq. (14), as presented in Yeoh [28]. This model falls under the phenomenological category and has been preferred due to its ability to minimize the average error for polyester fibers, as demonstrated in a similar implementation found in the literature by da Cruz [29].

$$W = C_1(I_1 - 3) + C_2(I_1 - 3)^2 + C_3(I_1 - 3)^3 + \left(\frac{C_4}{C_5}\right) \cdot \left(1 - \exp\left(-C_5(I_1 - 3)\right)\right) \tag{14}$$

The material parameters of the viscoelastic model (τ_i, γ) and the hyperelastic model (C_i) are obtained by a fitting curve procedure, where the numerical results, when compared to the experimental, should present small errors. A point-to-point percentage relative difference (RD) is used to quantify the error, and these relative differences compose an average error for the objective function.

3 Results

The result of the characterization of the SFS5202 polyester multifilaments is shown in Tab. 1.

Table 1. Mechanical results polyester SFS5202

Property	Test Result
Linear Density [dtex]	2266.8
Breaking Strength [N]	191.95
Elongation at Break [%]	13.73
Linear Tenacity [N/tex]	0.8468

In the loading and unloading (fatigue cycle), the control is by force. As stated in the methodology, the loading varies between 20% and 50% of the rupture value for each sample. In the case of the sub-rope test, force data acquisition and area estimation are combined to obtain tension-related data. On the other hand, measuring the area for the multifilament poses a challenge, so a mathematical approach is employed, which combines force values, specific mass (ρ), and linear density (ρ_L) to determine the tension (σ), as described in eq. (15).

$$\sigma[MPa] = \frac{F[N] \cdot \rho\left[\frac{g}{cm^3}\right]}{\rho_L\left[\frac{g}{m}\right]} \tag{15}$$

With the experimental stress data that adjust the numerical simulation for the last load cycle of the protocol presented in da Cruz et al. [24], is possible to carry out the numerical simulation. Below, the results are plotted in terms of experimental data (black dots), along with numerical simulation (blue curve), in Fig. 2 for multifilament and in Fig. 3 for sub-rope.

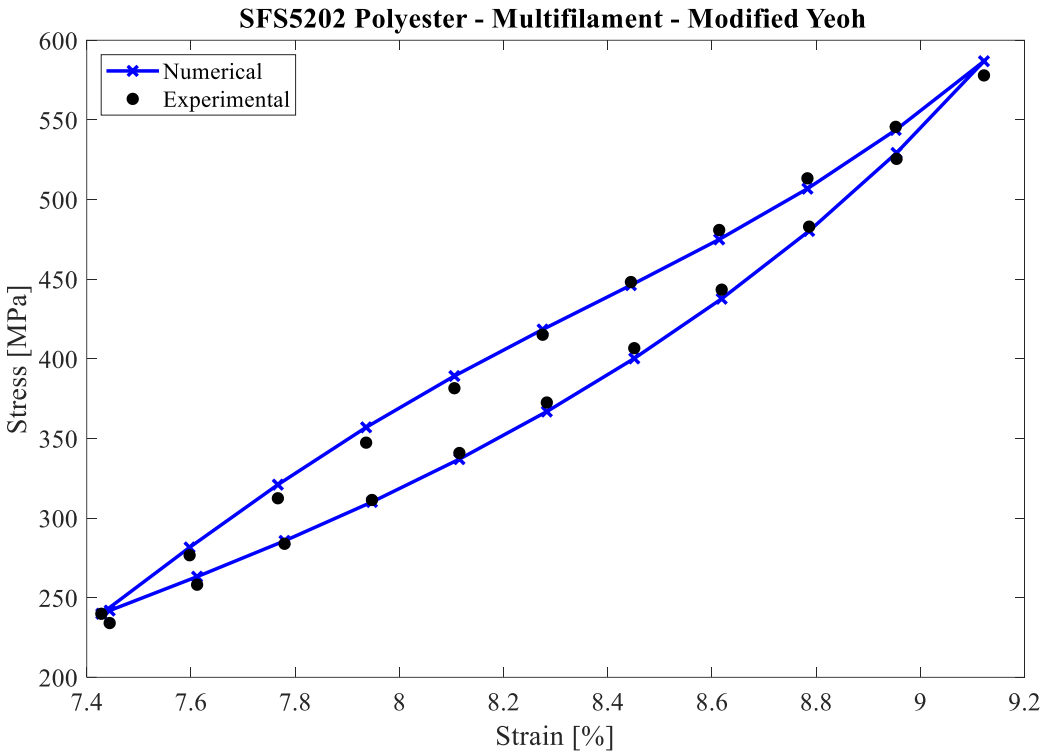

Figure 2. Numerical simulation result, multifilament

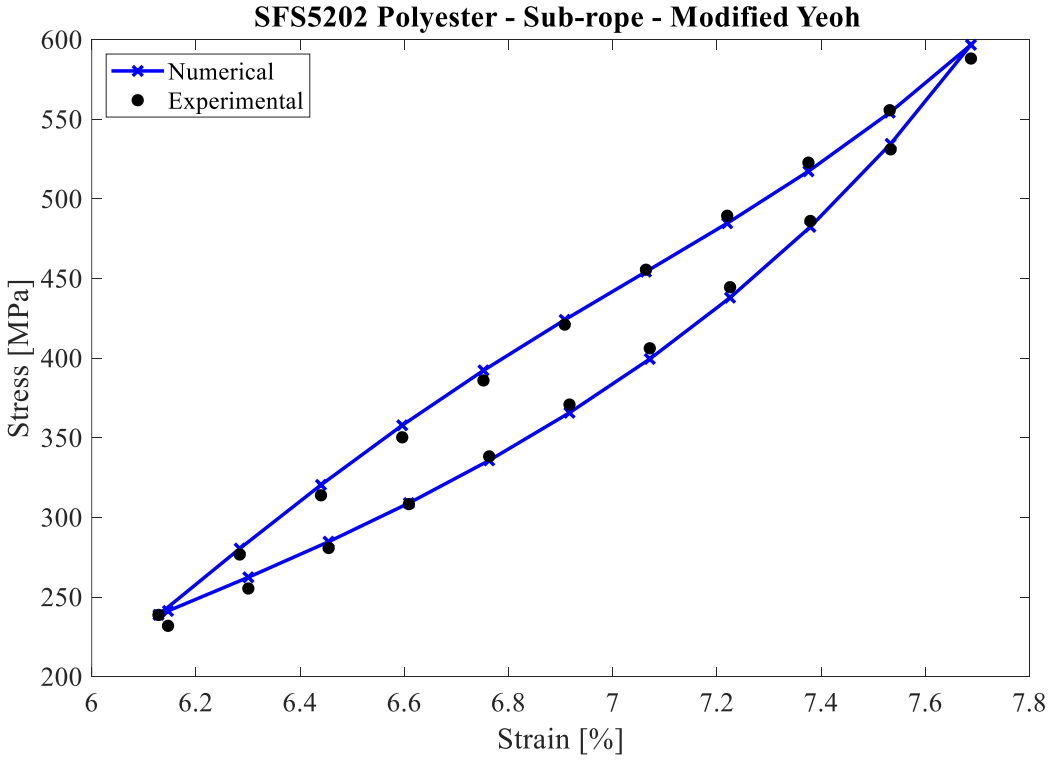

Figure 3. Numerical simulation result, sub-rope

The numerical simulation itself proves to be highly efficient, both in terms of visual and mathematical criteria,

with the average error for the multifilament simulation being 1.34% and for the sub-rope simulation being 1.28%.

The model constants obtained in the numerical simulation are shown in Tab. 2. The same table also presents a ratio between the values of multifilament and sub-rope. It is important to note that the first three constants described are in the same order of magnitude and exhibit good similarity, with ratios close to 1. However, the constants C2 and C5 are in different orders of magnitude (integer and decimal) and show slight differences when observing the ratios. As for constants C3 and C4, they demonstrate the most significant differences in the ratios, but it is important to highlight that the values for both samples and both constants are minimal (negligible).

Table 2. Strain energy function constants, Modified Yeoh

Constants	Multifilament	Sub-rope	Multifilament/Sub-rope
γ	0.500	0.500	1.000
τ	18.505	22.756	0.813
C_1	41.694	45.103	0.924
C_2	0.655	1.037	0.631
C_3	3.000E-08	1.000E-08	3.000
C_4	2.280E-06	2.900E-07	7.862
C_5	0.441	1.202	0.367

Regarding the differences in the values of the constants in the model, they indicate distinct constitutive behaviors. This observation is evident from the experimental values themselves, where similar stresses are noted, but the strains exhibit varying scales and gaps. Since these experimental data are utilized as adjustments for simulations, it is natural for some differences to arise in the constant values.

Despite these variations, specific values still exhibit similarities. It is possible that the differences in strain behavior are linked to the construction level, as sub-ropes undergo twisting and braiding. The braiding step often serves the purpose of constraining deformation precisely.

4 Conclusions

The results show that different construction levels can be adequately simulated, and their mechanical behavior remains representative. The variations in the model constants are attributed to the construction level, but the constitutive behavior remains dominant for the material.

There is a possibility that the strain energy model obtained for the multifilament can be adjusted using a formation law to approximate the behavior of the sub-rope. In the literature on offshore moorings with synthetic fibers, some authors indicate a correlation of properties between 65-75% between multifilament and rope.

Future studies, even exploratory at this stage, can be conducted to establish this formation law or degree of correlation between the numerical simulation for a multifilament and the adjusted expression to determine the constitutive behavior of a sub-rope. Setting up a database for different conditions of torsion and strand pitch in manufacturing the sub-rope would be essential for this purpose. Once this formation law is derived, it will apply to all interpolated conditions for that material.

Therefore, this study provides evidence of such a correlation and makes progress towards enabling the determination of the constitutive behavior in multifilament to predict the constitutive behavior of higher construction levels if they are made from the same material and manufacturing process.

Acknowledgements. This work has been supported by the following Brazilian research agencies: CAPES, CNPq and FAPERGS. We also thank for the financial support to the company Tecnofibers Desenvolvimento e Tecnologia Ltda.

Authorship statement. The authors hereby confirm that they are the sole liable persons responsible for the authorship of this work, and that all material that has been herein included as part of the present paper is either the property (and authorship) of the authors, or has the permission of the owners to be included here.

References

[1] G. P. Horn, J. Chaussidon, M. Obstalecki, D. A. Martin, P. Kurath, R. G. Backstrom, and S. Kerber, "Evaluating fire service escape ropes at elevated temperatures and fire conditions". *Fire Technology*, vol. 51, pp. 153-171, 2015.
[2] A. A. Leal, R. Stämpfli and R. Hufenus, "On the analysis of cut resistance in polymer-based climbing ropes: New testing methodology and resulting modes of failure". *Polymer Testing*, vol. 62, pp. 254-262, 2017.
[3] C. K. S. Pillai and C. P. Sharma, "Absorbable polymeric surgical sutures: chemistry, production, properties, biodegradability, and performance". *Journal of biomaterials applications*, vol. 25, n. 4, pp. 291-366, 2010.
[4] C. C. Chu, "Materials for absorbable and nonabsorbable surgical sutures". *Biotextiles as medical implants*, Woodhead Publishing, pp. 275-334, 2013.
[5] M. Tummalapalli, S. Anjum, S. Kumari and B. Gupta, "Antimicrobial surgical sutures: Recent developments and strategies". *Polymer Reviews*, vol. 56, n. 4, pp. 607-630, 2016.
[6] S. Gupta, V. K. Rao and J. Sengupta, "Evaluation of polyester fiber reinforced concrete for use in cement concrete pavement works". *Road materials and pavement design*, vol. 9, n. 3, pp. 441-461, 2008.
[7] L. Huang, X. Yang, L. Yan, K. He, H. Li and Y. Du, "Experimental study of polyester fiber-reinforced polymer confined concrete cylinders". *Textile Research Journal*, vol. 86, n. 15, pp. 1606-1615, 2016.
[8] D. K. Y. Tam, S. Ruan, P. Gao and T. Yu, "High-performance ballistic protection using polymer nanocomposites". *Advances in military textiles and personal equipment*, Woodhead Publishing, pp. 213-237, 2012.
[9] N. M. Nurazzi, M. R. M. Asyraf, A. Khalina, N. Abdullah, H. A. Aisyah, S. A. Rafiqah, F. A. Sabaruddin, S. H. Kamarudin, M. N. F. Norrrahim, R. A. Ilyas and S. M. Sapuan, "A Review on Natural Fiber Reinforced Polymer Composite for Bullet Proof and Ballistic Applications". *Polymers*, vol. 13, n. 4, id. 646, 2021.
[10] C. J. M. Del Vecchio, *Light weight materials for deep water moorings*. PhD thesis, University of Reading, 1992.
[11] D. Petruska, J. Geyer, R. Macon, M. Craig, A. Ran and N. Schulz, "Polyester mooring for the Mad Dog spar—design issues and other considerations". *Ocean Engineering*, vol. 32, n. 7, pp. 767-782, 2005.
[12] W. Huang, H. X. Liu, G. M. Shan and C. Hu, "Fatigue analysis of the taut-wire mooring system applied for deep waters". *China Ocean Engineering*, vol. 25, pp. 413-426, 2011.
[13] S. D. Weller, L. Johanning, P. Davies and S. J. Banfield, "Synthetic mooring ropes for marine renewable energy applications". *Renewable energy*, vol. 83, pp. 1268-1278, 2015.
[14] H. R. Aqdam, M. M. Ettefagh and R. Hassannejad, "Health monitoring of mooring lines in floating structures using artificial neural networks". *Ocean Engineering*, vol. 164, pp. 284-297, 2018.
[15] H. Saidpour, L. Li and R. Vaseghi, "The effect of rope termination on the performance of polyester mooring ropes for marine applications". *Ocean Engineering*, vol. 195, id. 106705, 2020.
[16] S. Xu, S. Wang and C. G. Soares, "Experimental investigation on the influence of hybrid mooring system configuration and mooring material on the hydrodynamic performance of a point absorber". *Ocean Engineering*, vol. 233, id. 109178, 2021.
[17] J. F. Beltran and E. B. Williamson, "Numerical simulation of damage localization in polyester mooring ropes". *Journal of engineering mechanics*, vol. 136, n. 8, pp. 945-959, 2010.
[18] W. Ouarhim, M. Ait-Dahi, M. O. Bensalah, M. El Achaby, D. Rodrigue, R. Bouhfid and A. Qaiss, "Characterization and numerical simulation of laminated glass fiber–polyester composites for a prosthetic running blade". *Journal of Reinforced Plastics and Composites*, vol. 40, n. 3-4, pp. 118-133, 2021.
[19] C. V. Amaechi, A. C. Odijie, F. Wang and J. Ye, "Numerical investigation on mooring line configurations of a Paired Column Semisubmersible for its global performance in deep water condition". *Ocean Engineering*, vol. 250, id. 110572, 2022.
[20] D. M. da Cruz, C. E. M. Guilherme, F. T. Stumpf, and M. B. Bastos, "Numerical Assessment of Mechanical Behavior of Mooring Lines Using Hybrid Synthetic Fiber-Rope Segments". In *Offshore Technology Conference (OTC 2023)*, 2023.
[21] J. C. Simo and T. J. Hughes. *Computational inelasticity*, vol. 7. Springer Science & Business Media, 1997.
[22] ASTM D1577. *Standard Test Methods for Linear Density of Textile Fibers*. American Society for Testing and Materials, West Conshohocken, 2018.
[23] ISO 2062. *Textiles — Yarns from packages — Determination of single-end breaking force and elongation at break using constant rate of extension (CRE) tester*. International Organization for Standardization, Geneva, 2009.
[24] D. M. da Cruz, A. Penaquioni, L. B. Zangalli, M. B. Bastos, I. N. Bastos and A. L. N. da Silca, "Non-destructive testing of high-tenacity polyester sub-ropes for mooring systems". *Applied Ocean Research*, vol.134, id. 103513, 2023.
[25] D. M. Cruz. *Estudo teórico, experimental e numérico do comportamento viscoelástico e caracterização de fibras sintéticas poliméricas*. Trabalho de Conclusão de Curso de Graduação, Universidade Federal do Rio Grande, 2022.
[26] P. Flory, "Thermodynamic relations for high elastic materials". *Transactions of the Faraday Society*, vol. 57, pp. 829-838, 1961.
[27] G. A. Holzapfel. *Nonlinear solid mechanics: a continuum approach for engineering science*. John Wiley & Sons, 2000.
[28] O. H. Yeoh, "Some forms of the strain energy function for rubber". *Rubber Chemistry and Technology*, vol. 66, n. 5, pp. 754-771, 1993.
[29] D. M. da Cruz, T. L. Popiolek Júnior, M. A. Barreto, C. E. M. Guilherme and F. T. Stumpf, "Avaliação de modelos de energia para simulação numérica do comportamento mecânico de multifilamentos de poliéster". *The Journal of Engineering and Exact Sciences*, vol. 9, n. 1, id. 15321-01e, 2023.